Draft version April 28, 2015
Preprint typeset using LaTeX style emulateapj v. 12/16/11
**Key Words** *Complexity, Spike, Cortex, Sleep, Seizure, Multielectrode, Neural Ensemble*



# MULTISCALE BALANCE OF EXCITATION AND INHIBITION IN SINGLE-UNIT ENSEMBLE RECORDINGS IN HUMAN AND MONKEY NEOCORTEX

Nima Dehghani [1,2] Adrien Peyrache [3] Bartosz Telenczuk [2] Michel Le Van Quyen [4] Eric Halgren [5]
Syd S. Cash [6] Nicholas G. Hatsopoulos [7] Alain Destexhe [2]

1. Wyss Institute for Biologically-Inspired Engineering, Harvard University, USA.
2. Laboratory of Computational Neuroscience, Unit de Neurosciences, Information et Complexit, CNRS, France.
3. NYU Neuroscience Institute and Center for Neural Sciences, New York University, USA.
4. Centre de Recherche de l'Institut du Cerveau et de la Moelle pinire (CRICM), UPMC, France.
5. Multimodal Imaging Laboratory, Departments of Neurosciences and Radiology, University of California San Diego, USA.
6. Department of Neurology, Massachusetts General Hospital and Harvard Medical School, USA.
7. Department of Organismal Biology and Anatomy, Committee on Computational Neuroscience, University of Chicago, USA.

*Draft version April 28, 2015*

## ABSTRACT

Neocortical ensemble recordings (human/monkey) were used to categorize units into regular-spiking and fast-spiking cells based on spike-waveform features and functional interactions. We adapted renormalization to evaluate the static/dynamic balance aspects between these cell groups. We found that the ensemble magnitude distribution is similar for both groups at multiple scales, demonstrating an overall balance. Scaling the ensemble series to a matrix of Excitation-Inhibition (E-I) ensemble pairs, enabled us to quantify the detailed dynamics of E-I in different states. Minor balance deviations were found in light slow-wave sleep (SWS), Rapid Eye Movement (REM), and wakefulness. Deep SWS showed moderate deviations from balance. These multiscale features were also found in a spiking neurons model of balanced states. In contrast, we observed a multiscale break-down of balance during focal seizure. Summarizing, neocortex shows an overall multiscale E-I balance across states, except seizures, showing that balanced E-I is a fundamental feature of normal brain activity.

## 1. INTRODUCTION

Balanced excitation/inhibition (E/I) is not only considered to be a functional cornerstone in the cerebral cortex, but also has been hypothesized to play a major role in areas other than cortex (Okun *et al.* 2010). The role of balance in neocortical processing was first suggested theoretically (Shadlen & Newsome 1994; Vreeswijk & Sompolinsky 1996). Later experimental evidence, in vitro (Shu *et al.* 2003) and in vivo (Haider *et al.* 2006) became the basis for the claim that a fundamental property of cortical processing lies in balanced inhibition and excitation. The concept of balanced networks was further extended to its influence on maximizing information capacity and information transmission in terms of neural avalanches (Shew *et al.* 2011; Lombardi *et al.* 2012).

The focus of this study is to investigate whether the inhibitory and excitatory systems interact in a balanced way at many temporal scales. Such possible multiscale aspect of neural computation, renders it as a reminiscent of state transitions in other physical systems, which also involve many different scales (Wilson 1979). Renormalization method, describes phase transitions by relying on spatial infinity of the system (Kadanoff *et al.* 1967; Wilson 1971, 1975). In analogy, a large ensemble of neural events provides the platform for dealing with infinity in the temporal domain, where instead of particles going through spatial distribution and phase transition, information in the system is conveyed by the temporal order of the neural packets and, hence, different states (of consciousness) emerge as the functional network constantly re-morphing itself.

Whether or not inhibitory and excitatory systems interact in a balanced way over many different scales of computation, is presently unknown. In this paper, we address this question by taking advantage of recent advances in the recording and separation between excitatory and inhibitory cells (Barthó *et al.* 2004; Peyrache *et al.* 2012) to characterize the dynamics of excitatory and inhibitory populations, in human recordings (temporal cortex), and monkey recordings (motor and premotor cortex). The units were initially clustered based on spike shape, and in a next step, their excitatory or inhibitory character could be confirmed by their functional interactions, as determined using cross-correlograms (Peyrache *et al.* 2012). To the best of our knowledge, this procedure provides for the first time in human, a coherent separation between the first categorization of human cerebral cortex ensemble unit activity into two groups of Fast-Spiking (FS) and Regular-Spiking (RS) cells (see McCormick *et al.* 1985; Barthó *et al.* 2004 for earlier implementation in animal experiments), where their putative excitatory or inhibitory nature could be shown through morpho-functional discrimination, i.e. spike-waveform characteristics in parallel to short-delay correlation modulation of pair neurons (see Peyrache *et al.* 2012 for details of the procedure). This was only possible because of the long period of the recordings (several segments of continuous 12-hour recordings for each subject). A similar discrimination between RS and FS cells was also done for the monkey recordings using a similar electrode array (Telenczuk et al., in preparation). Together, these human and monkey recordings provide a unique data set where one can investigate the dynamics of excitation and inhibition in different brain states. In the present paper, we characterize this dynamics by renormalizing the temporal structure of ensemble inhibi-

nima.dehghani@wyss.harvard.edu

tion and excitation, analyzing their interaction in different brain states and showing situations when the balance breaks down.

## 2. RESULTS

### 2.1. *Sample Recordings and categorization of cell population*

We first show the dynamic balance between excitatory and inhibitory cell activities in all different brain states, in human and monkey. We then use a number of methods to quantify this balance at different temporal scales, as well as the deviations from balanced activity. Finally, we show an example of a pathological brain state where the balance breaks down.

Figure 1 shows raw traces of local field potential (LFP) during slow-wave sleep (SWS) from both monkey and human. Along with the LFP, the rasters show the activity of single units divided into RS (blue) and FS (red) cells. We use this categorized ensemble activity to quantify the neocortical balance of excitation and inhibition.

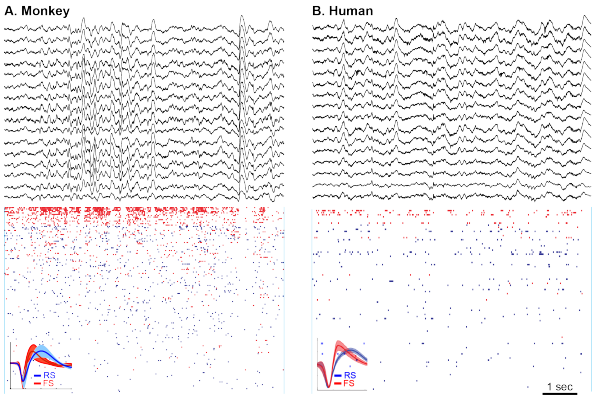


FIG. 1.— Sample recordings from a UTAH multielectrode array in Monkey (A) PMD and Human (B) Temporal cortices during 8 sec of SWS (Slow-wave sleep). In each panel, the upper section depicts LFP (local field potentials) from different locations of the multielectrode array. Lower sections show the corresponding Excitatory (blue) and Inhibitory (red) cells. Insets show the spike-waveform that was used to categorize the units into two inhibitory and excitatory cell populations.

### 2.2. *Recordings from different states are suggestive of excitatory and inhibitory balance*

A consistent observation for different states is that the inhibition and excitation mirror each other (Fig.2 and supplementary Fig.S1, note the normalized histograms of ensemble activity). One can see from the overall firing patterns (bottom), that in general an increase or decrease of the excitatory population is mirrored by similar dynamics among inhibitory cells, sometimes with a slight delay (see below for quantification).

Any choice of temporal scale for binning is somehow arbitrary. A further look at the example recordings in Fig.2 shows that in majority of the time, the two interacting ensembles follow the same trend at multiple scales and that deviations from perfect balance are more pronounced for the SWS. Additionally, it is noticable that sometimes the two ensembles follow each other at certain scales but not all (Fig.2, bottom traces, representing the

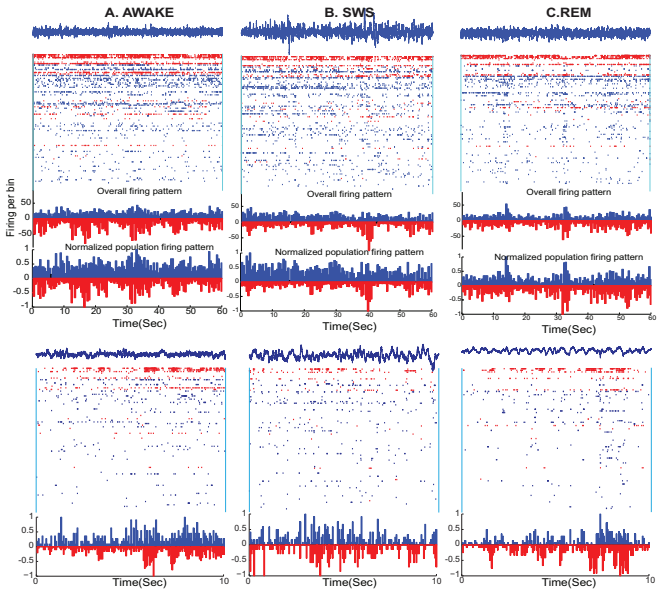


FIG. 2.— Sample recordings for awake (A), SWS (B) and REM (C) in human. Top row shows 60 second windows; bottom row shows a 10 second window of the same state. Putative inhibitory neurons (FS cells) are shown in red. Putative excitatory neurons (RS) are depicted in blue. At the top of each panel, a sample LFP trace (in blue) accompanies the spiking activity. Neurons are sorted based on their firing rate, within the portrayed epoch, in a descending order. Histograms show the overall activity of RS (blue) and FS (red) cells. In the normalized histogram, overall activity of each population is normalized to the maximum of firing rate (of the corresponding FS or RS population) in the shown example. Zero lag correlation values are respectively: 0.726, 0.47 and 0.503.

zscored addition of normalized excitatory (blue) and inhibitory (red) ensembles across the scales.). Similar patterns are observable in examples from monkey recordings (see Fig.S2).

This observation leads to question whether such possible overall balance extends throughout many periods, and at many time scales. Do the instantaneous fluctuations show balanced dominance. And, what happens when the system loses its capability to preserve balance between excitation and inhibition? In what follows, we aim to decipher such possible relations between excitation and inhibition and we provide a quantitative signature of probable multiscale balance.

### 2.3. *Dynamic and Static aspects of balance*

#### 2.3.1. *Preservation of balance across scales*

To test balance across multiple temporal scales, we defined 32 different scales ranging from a few milliseconds to many decades of seconds (as shown in Fig.4A). A multi-step zoom across some scales portrays that ensemble excitation and inhibition keep each other in an overall checked state at many lengths of computation. An example shown in Fig.4, panels C1 through C5, portrays that when the firing of a given category is normalized to the total related ensemble firing power, excitation and inhibition follow each other's fluctuations *en large* [1]

[1] When the E and I ensemble activity are normalized, they portray scaled mirror images of each other. As with any current ensemble recording we are subsampling the possible space of neurons, one can only extract estimates of balance rather than its exact magnitude. The true scaling of balance could only be calculated

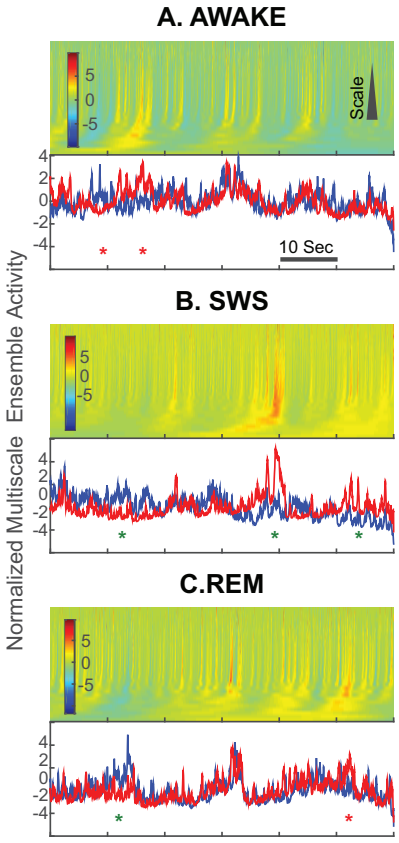


FIG. 3.— Multiscale features of excitation and inhibition balance in sample 60 seconds recordings (The examples are from Fig.1 panels A, B and C). Heatmaps at the top: Each row in the heatmap shows the normalized (zscore) difference of ensemble excitation and inhibition for a given scale. The scales are defined as in Fig.4, increasing from the top to bottom (from fine-grain to coarse-grain). The color saturation towards red signifies instantanous dominance of inhibition. Blue saturation shows instantanous dominance of excitation, while green shows tight match between normalized ensemble excitation and inhibition. Bottom traces show the zscored addition of normalized excitatory (blue) and inhibitory (red) ensembles across the scales. Red stars show where the two interacting ensembles do not show similar trends in their multiscale fluctuations. Green stars show times when ensemble excitation and inhibition follow each other at certain scales but not all. Any of these states leads to a multiscale deviation from perfect balance. Such deviations are more pronounced for the SWS (see Fig.8).

In Fig.4 C1-C5, the normalization is done to bring the mean to the same level for visual comparison of mirrored E-I fluctuations across scales. One of the key observations is that the standard deviation (and variance) of the system decreases (around the clamped mean) as one moves towards the coarse-grained time series. When examination of the fluctuation is extended to the whole recordings, by looking at the variance around the mean (i.e., coefficient of variation, CV), one observes the symmetrical decrease of CV across scales (Fig.S3A). Upon randomization and destruction of the E-I ensemble temporal relation, this symmetry is broken (Fig.S3B). This multiscale symmetric change of E-I fluctuations (CV), is accompanied by a multiscale unidirectional symmetry of the E-I ensemble pairs, aligning themselves with the perfect line of balance (see Fig.S3C as well as Fig.7A). The dispersion from the diagonal line of balance (of the unidirectional symmetry), shows a balanced instantaneous dominance of E and I systems, following the reduction of fluctuation around mean, as was discussed with CV (see Fig.S3D as well as Fig.S5C and Fig.6B). These evidences show that multiscale balance underlies the neural ensemble spiking pattern in the cerebral cortex. When the scale changes, the system shows self-similar behavior in terms of E-I fluctuations;i.e, the two ensemble E and I follow each other across many length scales of computation. This constitutes clear evidence for scale-invariance in terms of the correlated fluctuations of excitation and inhibition in cerebral cortex. It important to note that such a scale invariance is not equivalent to other hypothesized forms of invariance, such as self-organized criticality, which was found in vitro (Beggs & Plenz 2003)) , but was not found in the present recordings in human/monkey (Dehghani *et al.* 2012).

We also evaluated the behavior of the correlations between excitation and inhibition across different temporal scales. As shown in Fig.5, the ensemble FS and RS series showed well correlated dynamics. This type of ensemble correlation was observed across the multiple timescales. Further, the Monte Carlo randomization (four different types of randomization were implemented) showed that such correlation can not be due to aggregation of spike series into ensembles (For details of ensemble cross-correlogram and the randomization, see methods).

The observed ensemble temporal interdependence, was seen in different subjects with different number of FS and RS cells yet with the similar relative RS/FS count ratio of 4 to 1 (Fig.5A1-A4), was multiscale (Fig.5B1-B4), and was observed in all states (Fig.5C1-C4). The percentage of co-occurence of spikes (in the ensemble series) at the lag zero and the maximum observed percentage of co-occurence (whether that maximum was at lag 0 or not) showed a robust multiscale linear relationship. A linear fit to the pooled values of lag zero vs maximum observed correlation, yielded a cross-subject average of 0.9988±0.0134 for Awake, 0.9985±0.0147 for REM, 0.9985±0.0162 for light-sleep and 0.9977±0.02539 for slow-wave sleep. We wish to emphasize on two key findings: a) the maximum of the *ensemble* cross correlation is close to zero lag (note that this cross correlation is not calculated as an average of pair-wise cross-correlograms). Instead it represents the linear correlation of the two ensemble series (at different scales), on average, fire together and one cell population is not following the fluctuations of the group by some fixed delay. This does not necessitate the influence to be forced through a common input. b) another aspect is that as the data is coarse grained, the peak narrows and the higher correlation of the short delay shoulders (in comparison to long delays) dissipates. This phenomenon is equivalent to the the observation that instantaneous E-I relation (at the ensemble level) is more rigid at higher time scales (also see Fig.S3C,D, Fig.6B and Fig.S5C). In this experimental setting, it is not possible to discern whether the nature of such feature of ensemble correlation is a top-down process (imposed through nested frequency orchestration of spiking) or if it is an emergent property of the network, or both.

if and only if activity of all excitatory and inhibitory neurons are measured; a challenge that is not met with current technology but perhaps achievable in future.

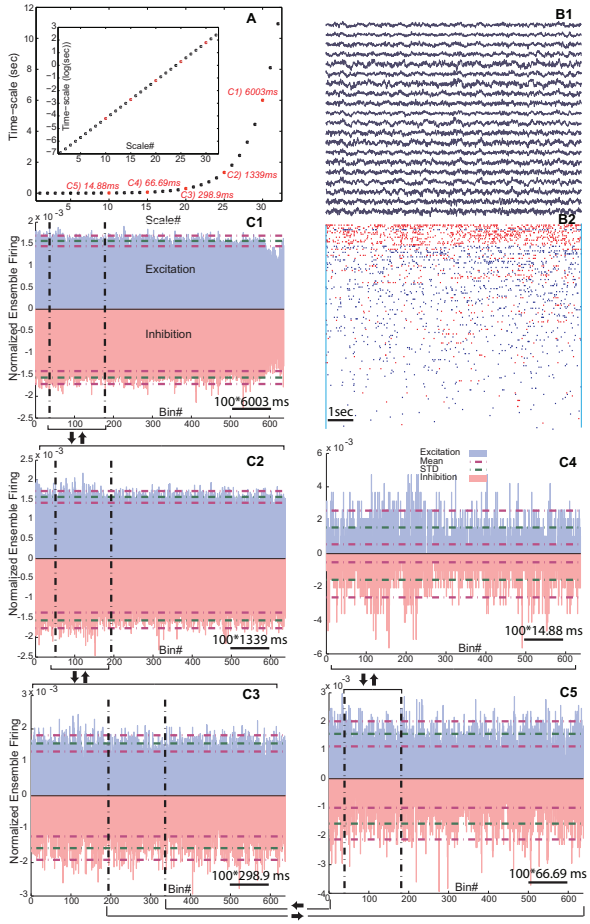


FIG. 4.— Preservation of excitatory-inhibitory balance across scales shows mirrored activity for different lengths of times (scales), in awake monkey. Note that the minus sign is only used conventionally to represent the opposing nature of excitation and inhibition. A. Definition of multiple scales used in the calculations. The scales were equally spaced in a logarithmic fashion. Those highlighted in red are shown in the example from monkey data in panels C1 through C5. Panels B1 and B2 show a sample 10 second of awake recordings' local field potential and ensemble spiking, respectively. In B2, as before, red units are FS (Fast-Spiking, putative inhibitory) and blue units are RS (Regular-Spiking, putative excitatory). Panels C1 to C5 show ensemble activity of excitation (blue) versus inhibition (red) at multiple scales. In each panel, the ensemble firing of a given cell category (FS or RS) is normalized by the total firing power in the same cell category during the shown epoch. For example, in panel C1 representing scale 30, each bin is about 6003 (ms) and total of 656 bins, show a duration of 1.0938 hr. Then a window of this epoch was chosen and zoomed in (scale 25) as shown in panel C2. The chosen window has exactly the same number of bins in scale 25. The ensemble firing of FS and RS in the 25th scale epoch was then normalized by the total firing of the FS and RS within this 656 bin epoch. Panel C3 to C5 are the next steps of zooming in (note the arrows showing the consecutive steps) the scales 20, 15 and 10. Again, in each step, exactly 656 bins of that scale are shown (and used for normalization). The mean and standard deviations are shown with dashed green and magenta lines, respectively. The ensemble activity shows a remarkable multiscale balance.

Multiscale distribution of magnitude and frequency of E-I ensemble fraction activity shows a general balance between the two interacting systems. This evidence for multiscale balance is depicted in Fig.6A. Whether in SWS or wakefulness, the two systems show an astounding symmetrical distribution of magnitude and frequency of the ensemble fraction of excitation and inhibition. The estimated cross-subject average skewness (of excitatory/inhibitory dominance), $\gamma = \mathrm{E}\left[\left(\frac{X-\mu}{\sigma}\right)^3\right]$, for different states were close to zero (in the case of absolute symmetry): -0.013±0.046 (awake), -0.012±0.087 (slow-wave sleep), -0.010±0.015 (light sleep) and 0.052±0.015 (REM). This symmetry shows that the balance is preserved across the scales. Naturally, as one approaches the coarse temporal scales, the distribution shrinks while still preserving the E/I balance (inset Fig.6B).

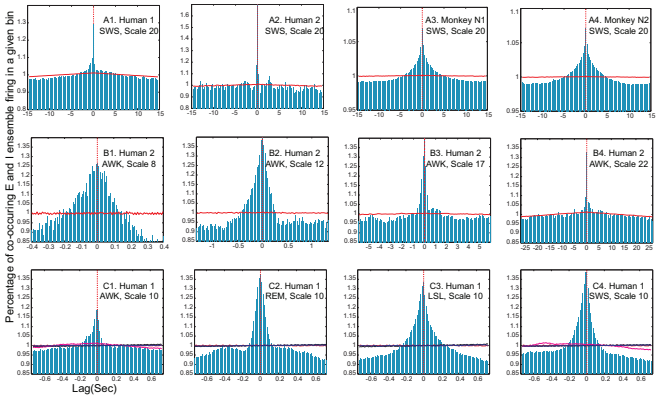


FIG. 5.— . Excitation and inhibition are correlated over multiple scales. In each panel, the cross-correlogram is shown as the histogram of delays of the spikes in the ensemble target series (inhibitory) with respect to the spikes of the reference series (excitatory). The vertical dashed line shows the lag zero, the horizontal line shows the average ensemble cross-correlogram of the Monte Carlo randomized process. In each histogram, the count of delays is turned into percentage (y-axis) for comparative reliability across different subjects (with different number of cells), different scales (different bin sizes) and different states (different length of the event). Note that in all panels lags -50 to +50 (bins) are shown. However, the span of time (x-axis, in sec) depends on the bin size of the evaluated timescale. A1 to A4, Ensemble cross-correlograms during slow-wave sleep across two different humans and two different nights of recording from the monkey are shown for a sample timescale. The shown randomized control (red) is the average of 100 realization of random permutation of the ensembles (see methods). B1 to B4, Ensemble cross-correlogram during wakefulness for a given subject across four different scales. Note that in each histogram of delays, the same number of lags (-50 to +50) are tested. For a given scale, the size of the bin relates to the temporal expanse of that scale (as defined in Fig.4. The randomized control (red) is the average of 100 rounds of realization of random local jitter (see methods for details). C1 to C4, Ensemble cross-correlogram of different states in another human subject for an example scale. All four randomized controls (horizontal lines) show similar outcomes. The randomized controls show that these four different randomization procedures yield highly reliable dispersion of events in the ensemble series such that the ensemble cross-correlogram no longer shows any temporal interdependency between the ensemble excitatory and inihibitory series.

If balance were to be dynamic, the neocortical computation should portray the capability of keeping the overall excitation and inhibition in check (as shown above) (Renart *et al.* 2010), while momentarily one cell population may dominate the other. As a result, the system should show moments of excitation dominance that are cancelled by moments of inhibition dominance and this feature should extend across all scales. The distribution of ensemble difference Fig.6B (as well as Fig.S3D and Fig.S5C) exactly exhibits this feature in a state-independent manner. Naturally, as one approaches the

larger scales, the extent to which the dynamic interplay fluctuates narrows. This follows the reduction of fluctuation around the mean as is portrayed by the symmetric changes of coefficient of variation (see Fig.S3A).

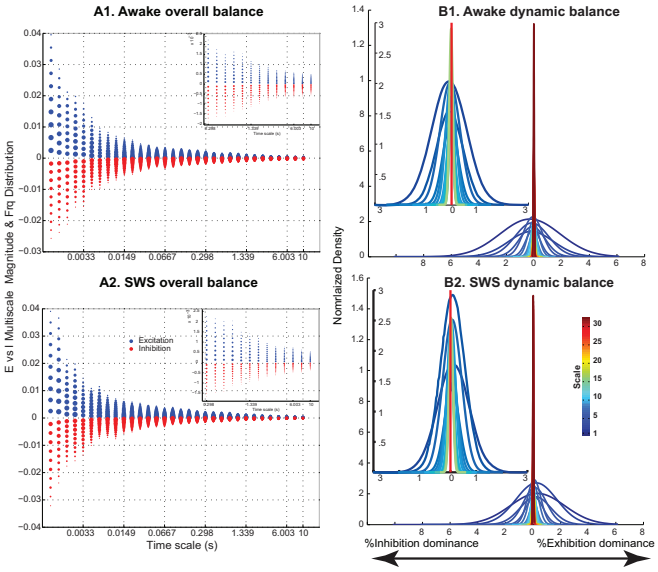


FIG. 6.— A1,2.Multiscale histogram of ensemble excitation (blue) versus inhibition (red) for the AWAKE and slow-wave sleep (SWS) in human A (Human REM and LSL (light sleep) as well as Monkey SWS and AWAKE had similar features, not shown here.). In each panel, there are 32 columns, each representing a given scale (as defined in Fig.4A). Each column represents the histogram of excitation (blue on top) and inhibition (red in bottom). The position of the circles refer to different magnitudes (increasing outward), and the diameter of each circle shows the frequency at which that given magnitude occurred. The insets are for the visualization of the higher scales, to avoid overplotting of red and blue circles. In all cases, a clear symmetry is observed across multiple scales. Mean absolute value deviation, $\frac{1}{n}\sum_{i=1}^{n}|x_i - \overline{X}|$, (a statistical measure of dispersion) for different states were 0.0023±0.0030 (awake), 0.0027±0.0034 (slow-wave sleep). Light sleep and REM, not shown here, had similar structure and statistical dispersion, 0.0021±0.0024 and 0.0028±0.0032 respectively. B1,2. Multiscale distribution of Excitatory versus Inhibitory dominance based on the dispersion from the diagonal line of unidirectional symmetry of the E-I ensemble pair scattering. In all different states, as the timescale increases, the magnitude of the ensemble fraction activity for both E and I become closer and closer to each other. The result is that while one system may still dominate, the deviation from absolute balance gets smaller and smaller. At the very high time-scales, while the distribution narrows, the shape of the distribution stays true to its features in the fine temporal scales. Note that the time-scales are color-coded (The insets show a zoom into higher scales).

These features of balance, i.e. overall multiscale balance and instantaneous dominance of ensemble excitation and inhibition in the light of preserved balance were also observed in a computational model of balanced states (see methods for the details of simulation). In the conductance-based (COBA) network of 4000 neurons (2000 inhibitory and 2000 excitatory neurons), the two population ensembles show a balanced mirrored activity (Fig.7A). Further examination of the two populations shows that the overall balance is preserved across multiple scales (Fig.7B, C and Fig.S4B). Similar to the experimental data, this is paralleled by the instantanous deviations from perfect balance (Fig.3, Fig.S2) and such observations are robust at many examined lengths of the data (Fig.4C).

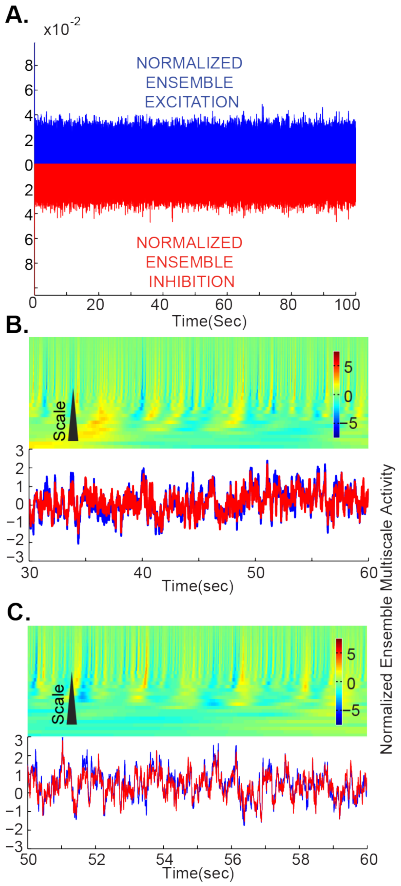


FIG. 7.— Multiscale balance in a computational model of AI (Asynchronous Irregular) states in networks of spiking neurons. A. As in Fig.4, preservation of excitatory-inhibitory balance across scales shows mirrored activity. B. As in Fig.3, the heatmap shows the normalized (zscore) difference of ensemble excitation and inhibition for multiple scales. Line traces show the zscored addition of normalized excitatory (blue) and inhibitory (red) ensembles across the scales. C. Same as B for a shorter period of time (last 10 seconds of B). These panels show that in general, the ensemble excitation and inhibition show an overall multiscale balance, even though there are instantanous deviations from perfect balance.

As shown in Fig.S5A1, even in the subsampled set, the paired E-I have a tight nearly symmetrical distribution along the diagonal line (line of perfect balance), showing the prescence of an overall balance. The multiscale balance in COBA network is destroyed (Fig.S5A2,3) by the same randomization methods that were implemented on the experimental data (see methods for details of randomization). Upon ensemble randomization, the alignment along the diagonal line morphs into a circular cloud representing noise). To see whether this behavior is an artifact of a given subsampled set, we ran a monte carlo resampling of the subsampled set (of 600 neurons). The results were the same, showing an overall balance across different scales. Additionally, in the 1000 iterations of the subsampled sets, the instantaneous dominance of ensemble excitation and inhibition shows a symmetric guassian feature (Fig.S5B) similar to that of the experimental data (Fig.6B). Average and individual density curves

of instantaneous dominance (thick dark lines and pale lines in Fig.S5C, respectively) are also in agreement with the experimental data in portraying the shrinkage of E-I dominance as one moves from fine temporal scales to coarse-grained ones (see also Fig.6B).

Although balance of E/I seem to be a hallmark of cortical computation, there is a large parameter space within which the input can be computationally processed while the balance is preserved (Xing & Gerstein 1996). While the distributions of ensemble fraction difference are more or less symmetric gaussian shaped, we have to emphasize that they do not follow normality in all cases. An example is shown in supplementary Fig.S6. If the data had come from a normal distribution, the values should follow the linear trend (shown in red). It is noticeable that in some cases, the tail ends deviate from normality and that the degree of this deviation is different from scale to scale. This deviation, which is further quantified in the text, could be due to reasons such as suboptimal sampling of units or more importantly the effects of slow oscillations on the spiking organization. Overall, the analysis shows that, although small deviations appear in deep SWS, the general balance was respected at all time scales examined here, and for all wake and sleep states. This aspect is further investigated in the next section.

### 2.3.2. *State-dependent properties of balance*

Though the system shows the core features of static and dynamic balance, our observations hint that departure from pure balance is an inherent feature of the system. We further quantified such departure based on the symmetry of the observations and that of the joint probability space. The complementary methods are shown in supplementary Fig.S7. Panel A, shows the implementation of weighted robust regression in order to calculate the angle between the symmetry axis of E-I ensemble activity vs the space axis of absolute symmetry. In parallel, we created a space in which for any given scale, the fraction of excitation, the fraction of inhibition, and their joint probability for all times t are morphed into a surface (supplementary Fig.S7B, C, D). Here, the deviation of the mid-plane of E/I ensemble activity from the plane of absolute symmetry is used to determine the degree of departure from absolute balance (see methods for details).

As mentioned above, deviations of E-I ensemble fraction activity from absolute symmetry are a core feature of dynamic aspects of multiscale balance. A nonparametric two-sample Kolmogorov-Smirnov test, $D_{n,n'} = \max_x |F_{AWAKE,n}(x) - F_{SWS,n'}(x)|$ where $F_{AWAKE,n}$ and $F_{SWS,n'}$ are the empirical cdfs (empirical cumulative distribution function) of the normalized E/I ratio distributions for the two states, rejected ($P_{val} \ll 10^{-3}$) that they come from the same distribution at the significance level of $\alpha = 0.01$. This shows that the degree of balance deviation is state-dependent. As portrayed in the Fig.8, the highest degree of deviation from perfect balance happens during SWS.

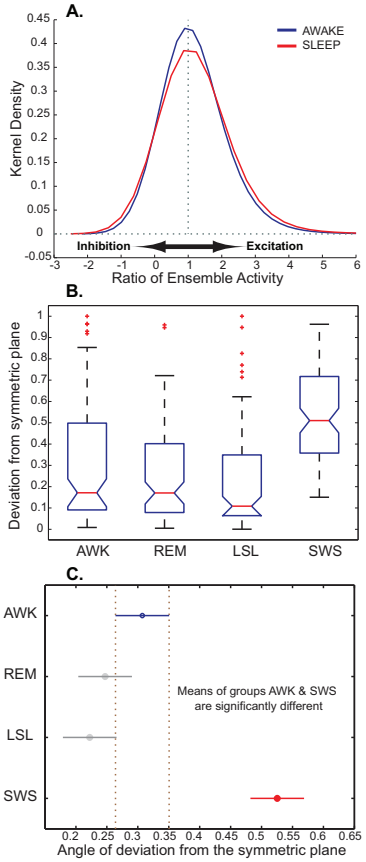


FIG. 8.— Panel A, kernel density of the ratio of E/I for the monkey awake and sleep states. Perfect balance (where the magnitude of ensemble matches) would be represented by the vertical dotted line (= 1). Though the qualitative symmetry in each state is preserved, the kernel density estimates of sleep and awake do not match, with more kurtosis in awake and broader shoulders in sleep. A Two-sample Kolmogorov-Smirnov test on the E/I ratio at the significance level of $\alpha = 0.01$, rejected ($P_{val} \ll 10^{-4}$) the null hypothesis that the data in awake and sleep are from the same continuous distribution. This is matched with the observations in humans, where the angle of deviation from the symmetric plane/axis is more pronounced during sleep rather than in awake (panel B). In the boxplot, the notch represents the median, the box boundaries show the lower and upper quartile and the asterix show the outliers. In a multiple comparison test, panel C, awake and sws show statistically significant differences between their means ($P_{val} \ll 10^{-3}$). Note that only slow-wave sleep shows significant statistical difference with the other states at $\alpha = 0.05$.

This higher degree of deviation from balance during sleep could be attributed to the fluctuations of inhibitory/excitatory activity during up-state and down-state (Renart *et al.* 2010; Steriade *et al.* 1993; Shu *et al.* 2003; Xue *et al.* 2014), as hallmarks of a bistable regime where toggling between the two states is enforced by the mutual excitation and feedback inhibition (Wilson & Cowan 1972). Transient stability of both up and down states is the other side of the coin characterized by a rhythmic transition between quiescent and active states (Holcman & Tsodyks 2006). This property, leads to the observed higher degree of deviations from absolute balance plane.

## 2.4. *E/I imbalance during seizures*

It has been speculated that the breakdown of the equilibrium between excitation and inhibition could lead to epilepsy. The idea that the lack of inhibition or excess of excitation can cause seizure is not a new one (Symonds 1959). This has been experimentally used to induce or control seizures, such as for example by inducing inhibition using optogenetics (Krook-Magnuson *et al.* 2013; Paz *et al.* 2013; Tø nnesen *et al.* 2009). Other optogenetic studies have related cortical E/I imbalance to other diseases such as mood disorders as well (Yizhar *et al.* 2011). However, it has been argued that such a clear-cut idea of lack of inhibition or excess inhibition as the major frame of epileptogenesis is perhaps misleading (Engel 1996).

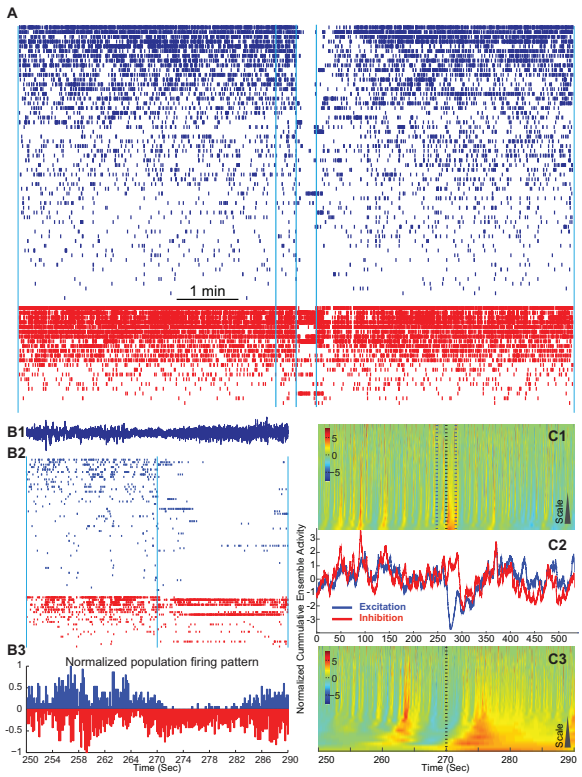


FIG. 9.— Misbalance in an example seizure recording in human. Panel A shows a 9 minute recording. Panels in B are the zoomed in version (the middle 40 seconds) of the same epoch (shown with the vertical lines in A). RS cells are in blue and ranked based on their firing rate within this epoch. Red cells show FS cells and are ordered according to their class firing rate. B1, LFP activity in the zoomed period, corresponding to B2 raster of FS and RS cells. B3, Normalized mirrored histogram showing where the misbalance occurs. C1. Heatmap of the normalized ensemble excitatory and inhibitory differences, corresponding to the 9 minute recording shown in A (Dotted lines mark the boundary of B1-3 and C2-3). C2. Normalized cummulative ensemble actvity of excitation vs. inhibition during the 540 seconds epoch. C3 is the zoomed in version of the middle 40 seconds (corresponding to panels in B and the marked are by dotted lines in C1). Seizure happens around the mid-point and is visually distinct from the rest of the recording. During the seizure, a clear misbalance occurs; however it shows complex multiscale characteristics. See Fig.S8 for more examples.

Here, we provide an example of a seizure recorded in one of our patients and show how E/I balance changes in a complex fashion that is in contrast to the simple misbalance scenario described above (see Fig.9A,B). During the seizure some excitatory cells and some inhibitory cells increase their firing while some decrease or even stop firing (Truccolo *et al.* 2011) yet an overall imbalance persists throughout the event. The same multiscale breakdown of the balanced excitatory-inhibitory activity was observed for all six seizures from two human patients. For additional examples, see Fig.S8. To further ealborate on the quantification of misbalance during seizing, we tested the dynamics of the multiscale features of ensemble excitation and inhibtion throughout the seizure. In the example seizure (shown in Fig.9), there is a complete break-down of the balance, were the inhibitory cells initially dominate, which is further followed by re-emergence of balance toward the end of this seizure episode. Heatmaps of difference of normalized (zscored) ensemble excitation and inhibition, Fig.9C1,C3 and multiscale line plot of normalized ensemble excitation and inhibition (Fig.9.C2), show that the interplay between the two populations harbors a multiscale feature during the misbalance.

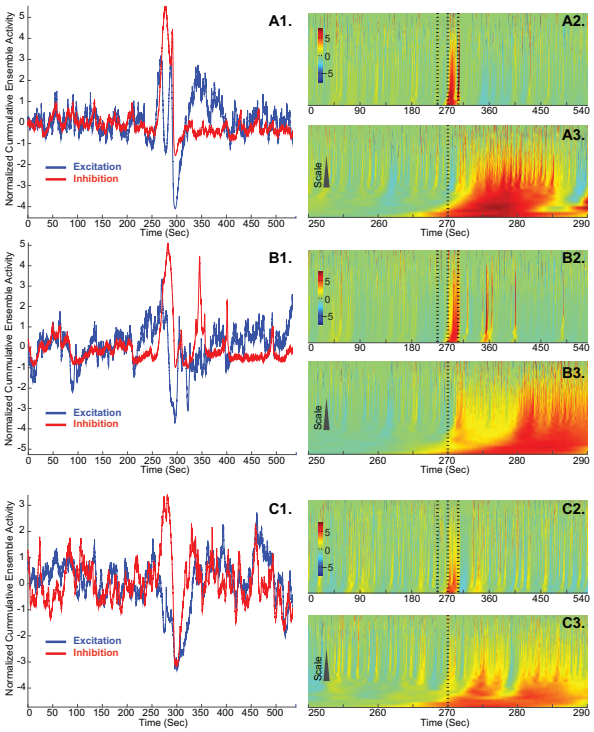


FIG. 10.— Break down of E/I balance in different seizure episodes. A1, B1 & C1. Multiscale features of balance breakdown during seizure. Blue and red traces show the normalized cummulative activity of ensemble excitation and inhibition across multiple scales (similar to Fig.3 bottom panels). In the shown examples (as well as in Fig.9), electergraphic seizure starts around 270 sec. In all cases, ensemble excitation and inhibition follow the same multiscale trend. At the time of seizure, the two ensembles go through major fluctuations, and disentangle. In C1, return to multiscale balance trend happens fairly shortly. In A1, the system returns to balance a bit later (around second 400) and in B1, the system shows prolonged distrubed balance in the examined period shown here. Panels A2:3, B2:3 and C2:3 show the heatmap of the normalized ensemble excitatory and inhibitory differences, corresponding to the 9 minute recording and the middle 40 seconds zoom in (similar to Fig.9C).

Similarly, in other examples in Fig.10, the two ensem-

bles follow similar multiscale trends up to the seizure initiation ( second 270), when suddenly the two systems become disengaged and fluctuate without any further interdependence. Such imbalanced fluctuation is later diminished and the two ensembles find their way to flow with the same multiscale trend again. Though this return to the balanced trend does not show any universal time scale. In some cases (Fig.9C, Fig.10D) it happens faster than others (Fig.10A) and in some cases (Fig.10B), it may not happen for even few minutes after the seizure has, electrographically, ended.

Note that the particular features illustrated here, such as the transient dominance of inhibition, may not be representative of all types of focal seizures. As these types of ensemble recordings become more abundant in clinical settings, in near future, it will become possible to test the multiscale features of balance in different types of seizures with the methods described here.

## 3. DISCUSSION

In this paper, we took advantage of the recent advances in the separation of excitatory and inhibitory cells, which were confirmed by direct cell-to-cell interaction (Peyrache *et al.* 2012). Our present analysis demonstrates that the excitatory and inhibitory neural populations are balanced in two cortical areas of human and monkey as well as in a COBA (conductance-based) network model with AI (asynchronous irregular) properties. This overall balance extends to multiple scales, as shown by the distributions of ensemble magnitudes (see Fig.4, Fig.7, Fig.6A and Fig.S5). We also found that the balance extends to nearly all brain states, and breaks down during epileptic seizures (Fig.9 and Fig.10). The network recovers from the multiscale breakdown of balance after the end of the seizure, albeit with no apparent universal time scale. This breakdown suggests that the balance of excitatory and inhibitory activities is important for normal brain function and sleep. It also provides an important indication that our discrimination between RS and FS cells leads to two functionally distinct populations of neurons, that can be balanced or unbalanced depending on brain state.

In the past, some have adapted methods like Ising model to describe the temporal structures of ensemble spiking (Schneidman *et al.* 2006) and others have tried to interpret neural information in the light of self-organization based on power-law structure of spiking or local field potential (Beggs & Plenz 2003; Petermann *et al.* 2009). However, these approaches suffer from bypassing certain complexities of the system: i.e the constantly interacting excitation and inhibition as well as possible clue to multifractality of system (Dehghani *et al.* 2012). It has been hypothesized that brain organization follows small-world networks Sporns & Honey (2006), but such view stays short of describing the complexity as seen in diversified variability of oscillatory graphoelements, such as thalamocortical spindles (Dehghani *et al.* 2010b,a). In contrast, descriptions based on computation in stochastic networks states (Destexhe & Contreras 2006) and those which harbour the dynamic balance of excitation and inhibition (Amit & Brunel 1997; Brunel 2000), provide a platform that could point to the observed complexity of the system. In the past, by studying the micro-circuitry of cortex at different states (wakefulness/drowsiness, light and deep slow-wave sleep), we have shown how spatiotemporal dynamics feature distance-dependent correlation, in the case of excitation, and a tight spatial correlation and temporal autocorrelation, in the case of inhibition (Peyrache *et al.* 2012). In a recent study, we also showed that a single scaling exponent can not sufficiently reporduce the ensemble complex dynamics (Dehghani *et al.* 2012). In the current study, we aim to bridge the existent gap between these notions by analyzing the balance of excitation and inhibition at many time scales during different states. Instead of staying limited to the pair-wise or higher order correlations (Peyrache *et al.* 2012; Schneidman *et al.* 2003; Shimazaki *et al.* 2012) or relying on the fundamental limitations of studying avalanches, we adapted renormalization to the temporal structure of ensemble inhibition and excitation, used the detailed quantification of their interaction at different states to show features of multiscale balance and showed that when the balance breaks down, seizure emerges. Previous in vitro observations support our findings that seizure emergence is not due to pure lack of inhibition or excess of excitation (see (de Curtis & Gnatkovsky 2009)).

The multi-scale characteristics of E/I suggests that the system is more complex than a a rigid system with perfect balanced activity. In fact, it has been shown that the spike timing itself seems to be finely tuned by dynamic interactions between excitatory and inhibitory conductances (Higley & Contreras 2006; Rudolph *et al.* 2007). In other words, the state of the system at a given point defines its capacity for responding to incoming stimuli. At fine time scales, the system may momentarily show either inhibitory or excitatory dominance (as in Fig.6A). However, the overall balance is always preserved, and this is true for wakefulness, REM or NREM sleep. Such properties also show that the system is not dominated by particular periodicities but seems to be broad-band (Fig.8). Naturally, as we move toward coarser and coarser time scales, the system becomes more and more rigid to the point that the gaussian shaped curves collapse and approach zero, i.e. equal power. It would be interesting to further characterize this momentary imbalance in future work, and the possible behavioral correlates of such imbalance.

Balance of excitation and inhibition has gone through many different renditions (Okun & Lampl 2009), from simulations based on random walk models (Gerstein & Mandelbrot 1964), to opposing views of balanced synaptic input (Shadlen & Newsome 1994; Softky & Koch 1993) and later to those relating it to synchrony (Stevens & Zador 1998), and those providing intracellular evidence for dynamic interplay between inhibition and excitation (Rudolph *et al.* 2007; Monier *et al.* 2008). However, for the first time, we show evidence of E/I balance in terms of network activity, estimated from large ensemble of units. The law of requisite variety expresses that high number of states of control elements are required to keep the controlled system in lesser number of stable states Ashby (1958). In complex systems, both scale and variability are necessary to keep a system in stable modes of operation and at every scale, variability is a must to provide adaptability (Bar-Yam 2004). The dynamics we see here seem consistent with such complex systems.

### 3.1. *Conclusion*

We suggest that the nervous system resides at a unique position in its state space, where unit firing in cortex, during wakefulness and sleep, reflects an overall preserved excitation-inhibition balance, but with highly rich dynamics across multiple temporal scales. This balance can tip one way or the other, and depending on the state of the system, can deviate from balance with different degrees of intensity. While the balance perturbation happens more regularly at finer temporal scales, it also transcends to other temporal scales of the system in a state-dependent fashion. When this multiscale dynamic balance breaks down, complex disorders such as epilepsy emerge. This is the signature of a system with many computational length scales, lending itself to a form of multiscale invariance.

## 4. METHODS

### 4.1. *Recordings*

Recordings of the ensemble neural activity were obtained through the implants of multielectrode arrays (Neuroport/Utah electrodes, Blackrock Microsystems). These arrays are composed of 100 electrodes arranged in a 10x10 matrix with an inter-electrode distance of 400 microns. For more details on electrodes see (Campbell *et al.* 1991; Jones *et al.* 1992). The patients, who were implanted, suffered from intractable seizures and were under neurosurgical monitoring to localize the focus of their epileptic seizure. The electrodes tips reached layer III of the neocortex (For details of implants see, (Truccolo *et al.* 2011). In the monkey, the implant was in the dorsal premotor cortex (PMd). Recordings were made during the performance of a motor task as well as during sleep. For details of implantation see (Dehghani *et al.* 2012; Truccolo *et al.* 2010). For the human studies, patients were given consent forms with detailed desciption of the purpose of the study and its potential risks. Approval for all human experiments involving recordings of single unit activity in patients was granted by the Institutional Review Boards of Massachusetts General Hospital / Brigham & Womens Hospital in accordance with the Declaration of Helsinki and required informed consent from each participant. For the primate experiments, all of the surgical and behavioral procedures were approved by the University of Chicagos IACUC and conform to the principles outlined in the Guide for the Care and Use of Laboratory Animals (NIH publication no. 86-23, revised 1985; IACUC Approval number: 71565).

As has been described previously, the spikes of putative excitatory (Regular Spiking., RS) neurons tend to be broader than putative inhibitory (Fast Spiking., FS) neurons (McCormick *et al.* 1985; Barthó *et al.* 2004). The recordings, were then spike-sorted and the units were categorized as either RS or FS. This categorization was based on morpho-functional characteristics of the spike-waveform and putative mono-synaptic connections (for details of such techniques see (Barthó *et al.* 2004; Peyrache *et al.* 2012). A Variety of extracted features describing the shape of the average spike waveform were used, such as half-width of the positive peak, half-width of the negative peak, interval between negative and positive peaks (valley-to-peak) and the ratio of the negative to positive peak amplitude. Based on these parameters, we classified the spike waveforms of all neurons into two groups using a standard K-means clustering algorithm. The procedure was repeated for each recording session separately; the neurons that were not assigned consistently to the same group were removed from further analysis.

### 4.2. *Multiscale temporal rescaling*

We used 32 different time scales to remap the ensemble activity to renormalized time-series of excitation and inhibition. For this process, spikes of ensemble excitatory group were binned at different time-scales. As the number of excitatory and inhibitory neurons in each recording differs from one another (even though their relative size 4/1, is close to the anatomical observations), these values were normalized by the number of the neurons in each category of cells to obtain the ensemble fraction. This condition would overcome the limitations arising from both sub-sampling (here, 100s of neurons out of many thousands) and spatial non-uniformity of sampling (although the recording electrode is a regular grid, unit recordings are not always regularly spaced). The same process was repeated for inhibitory neurons. The results yielded ensemble fractions of inhibition and excitation at many different time scales. These time scales were distributed with regular spacing in logarithmic scale, ranging from ms to 10s of seconds. The logarithmic scale was chosen to have denser distribution at finer temporal resolution and avoid the computational redundancy at the very coarse-grained level.

### 4.3. *Ensemble cross correlation*

We first created the ensemble pool of the FS and RS cells in each subject of the study. The two series were lined up temporally along a common time axis. The ensemble RS and FS cells were used as the reference and target series respectively. For a given temporal scale, the bin length was defined according to the size of that scale as in Fig.4A. For each spike in the reference ensemble series, the delays of the spikes in the target ensemble series within -50 to +50 bin lags were calculated. Next, the collective count of target spikes within a given lag was defined as the value of ensemble cross-correlogram between FS and RS series. This value was turned into a percentage for enabling the comparison across subjects with different number of neurons, multiple scales with a different number of aggregate of spikes, and different states with different duration of events. This process was realized for all scales.

#### 4.3.1. *Randomization*

Randomization was used to construct control for the ensemble cross-correlogram. We used four different systems of randomization to test for different within and between aspect of ensemble series. Any of the randomization protocols was realized 100 times. For each randomization category, the average of 100 random ensemble cross-correlogram was used as the control for verification of the observed patterns in the non-randomized cross-correlogram.

- *Random permutation of ISI in the ensemble series.* After pooling all the FS and RS cells into their ensemble series, the ensemble ISI (inter-spike interval) was calculated. Then, for each of the two ensemble series, a random permutation of its ISI was followed by cumulative summation of ISI, resulting in the new temporal order of ensemble spikes. This procedure guarantees that the randomized ensemble series has the exact number of spikes and exact set of ISIs as of the original ensemble series, albeit with different temporal arrangement of spikes within a given ensemble series.

- *Circular shift of spike ensemble.* In this type of randomization, the spikes were first pooled to create the ensemble FS and RS series. For each series, the ISI of the ensemble series was calculated. Then all the spikes in each series were shifted at once with a random value between the lower bound (1) and upper bound (maximum of the ISI in the ensemble series). In each randomization trial, it was made certain that the degree of the shift was not equal for the two FS and RS ensemble, guaranteeing that the temporal relation of the two series was never repeated. In contrast to the previous procedure (random permutation), this randomization kept the temporal of order of spikes within each ensemble series same as the non-randomized series. However, here the temporal relation of the two FS and RS ensembles was disrupted.

- *Fixed-ISI circular shift of spikes.* Before aggregating the spikes into the ensemble series, the ISI of each unit's spike series was calculated. Then the spikes of the unit were shifted based on a random value drawn between the lower bound (1) and upper bound (maximum of the ISI of the that unit's spike series). Next, all the randomized units were aggregated to create the randomized ensemble series. This procedure guarantees that the resultant ensemble series is constructed from units with intact internal structure of their spike timing but with a disrupted between-unit timing.

- *Local jitter randomization of spikes.* Next we tested the effect of randomization based on the statistics of each individual neuron before their aggregation to the ensemble series. First, the ISI of each FS (or RS) unit was calculated. Then the pool of the ISI as well as the ensemble of FS and RS was created. Next, each spike in the ensemble was shifted according a random number which was generated as the standard deviation plus a randomized (between -1 and 1, not including 0) multiple of the mean of pooled ISI. If the drawn random value was negative, the spike was shifted to the left and if the random chosen value was positive, the shift was toward the right in the ensemble series. This randomization, guarantees a tightly regulated data-driven local randomization based on the statistical properties of individual spikes.

### 4.4. *Deviation from absolute symmetry*

We used complementary methods to calculate the deviation from symmetry between excitatory and inhibitory activities. First, we estimated the data-derived axis of symmetry based on the weighted bisquare robust regression. Then the angle between this axis and the identity line was used to represent the degree of deviation from pure symmetry. In parallel, for each time-scale, and for a given state, the time series of ensemble spiking data were reshaped into a 3-dimensional surface where the dimensions were the fraction of excitation, the fraction of inhibition, and number of their occurrences. As the durations of different states (SWS, REM, Wakefulness) differ from each other, the joint probability of ensemble fractions were also normalized by the whole length of the state to provide comparable results for further quantifications; i.e., the result is a surface in the 3D space of the fraction of excitation, the fraction of inhibition, and their joint probabilities. Theses surfaces were then Z-scored and their major orientation axis was calculated. Then the mid-point of the iso-surfaces along the major orientation axis was defined. Using orthogonal regression, a plane was fit to these point along the major orientation axis. This plane, is the plane of approximate symmetry of the data and divides the surface into two halves. In case of absolute balance at a given scale, the plane of symmetry of data would coincide with the symmetry plane of the 3D space. Deviations from perfect balance was calculated using the dihedral angle between the symmetry plane of data and symmetry plane of the 3D space. The results of the dihedral rotation was similar to the angle between axis of symmetry and the weighted least square regression (using robust bi-square fit) of the data in the 2D rendering of excitation fraction and inhibition fraction.

### 4.5. *Computational model*

Network simulations were done using networks of excitatory and inhibitory spiking (integrate-and-fire type) neurons with sparse random connectivity (2000 excitatory and 2000 inhibitory neurons with 5% connection probability), and with conductance-based (COBA) synaptic interactions (See Fig.S4A). Such COBA networks were shown to display self-sustained asynchronous irregular (AI) balanced states ((Vogels & Abbott 2005); see this references for details of the parameters and see (Brette *et al.* 2007) for codes. The network activity was entirely self-sustained (no added noise), after a kickoff random stimulaton to initiate the AI state.

## 5. ACKNOWLEDGEMENTS

Nima Dehghani is an institute fellow of the Wyss Institute for Biologically-Inspired Engineering at Harvard Univerity; he was previously funded by the Ecole de Neuroscience de Paris (ENP). The research was funded by Centre National de la Recherche Scientifique (CNRS, France), Agence Nationale de la Recherche (ANR, France), European Community Future and Emerging Technologies program (BrainScales FP7-269921; The Human Brain Project FP7-604102) and National Institutes of Health (NIH grants 5R01NS062092, R01EB009282 and R01NS045853).

REFERENCES


Amit, Daniel J, & Brunel, Nicholas. 1997. Model of global spontaneous activity and local structured activity during delay periods in the cerebral cortex. *Cerebral cortex*, **7**(3), 237–52.

Ashby, William. 1958. Requisite Variety and its implications for the control of complex systems . *Cybernetica*, **1**(2), 83–99.

Bar-Yam, Yaneer. 2004. Multiscale variety in complex systems. *Complexity*, **9**(4), 37–45.

Barthó, Peter, Hirase, Hajime, Monconduit, Lenaíc, Zugaro, Michael, Harris, Kenneth D, & Buzsáki, György. 2004. Characterization of neocortical principal cells and interneurons by network interactions and extracellular features. *Journal of neurophysiology*, **92**(1), 600–8.

Beggs, John M., & Plenz, Dietmar. 2003. Neuronal Avalanches in Neocortical Circuits. *J. Neurosci.*, **23**(35), 11167–11177.

Brette, Romain, Rudolph, Michelle, Carnevale, Ted, Hines, Michael, Beeman, David, Bower, James M, Diesmann, Markus, Morrison, Abigail, Goodman, Philip H, Harris, Frederick C, Zirpe, Milind, Natschläger, Thomas, Pecevski, Dejan, Ermentrout, Bard, Djurfeldt, Mikael, Lansner, Anders, Rochel, Olivier, Vieville, Thierry, Muller, Eilif, Davison, Andrew P, El Boustani, Sami, & Destexhe, Alain. 2007. Simulation of networks of spiking neurons: a review of tools and strategies. *Journal of computational neuroscience*, **23**(3), 349–98.

Brunel, Nicolas. 2000. Dynamics of Sparsely Connected Networks of Excitatory and Inhibitory Spiking Neurons. *Journal of Computational Neuroscience*, **8**(3), 183–208.

Campbell, Patrick K., Jones, Kelly E., Huber, Robert J, Horch, Kenneth W., & Normann, Richard A. 1991. A silicon-based, three-dimensional neural interface: manufacturing processes for an intracortical electrode array. *IEEE transactions on bio-medical engineering*, **38**(8), 758–68.

de Curtis, Marco, & Gnatkovsky, Vadym. 2009. Reevaluating the mechanisms of focal ictogenesis: The role of low-voltage fast activity. *Epilepsia*, **50**(12), 2514–25.

Dehghani, Nima, Cash, Sydney S, Chen, Chih C, Hagler, Donald J, Huang, Mingxiong, Dale, Anders M, & Halgren, Eric. 2010a. Divergent cortical generators of MEG and EEG during human sleep spindles suggested by distributed source modeling. *PloS one*, **5**(7), e11454.

Dehghani, Nima, Cash, Sydney S, Rossetti, Andrea O, Chen, Chih Chuan, & Halgren, Eric. 2010b. Magnetoencephalography demonstrates multiple asynchronous generators during human sleep spindles. *Journal of neurophysiology*, **104**(1), 179–88.

Dehghani, Nima, Hatsopoulos, Nicholas G, Haga, Zach D, Parker, Rebecca A, Greger, Bradley, Halgren, Eric, Cash, Sydney S, & Destexhe, Alain. 2012. Avalanche Analysis from Multielectrode Ensemble Recordings in Cat, Monkey, and Human Cerebral Cortex during Wakefulness and Sleep. *Frontiers in physiology*, **3**(jan), 302.

Destexhe, Alain, & Contreras, Diego. 2006. Neuronal computations with stochastic network states. *Science (New York, N.Y.)*, **314**(5796), 85–90.

Engel, Jerome. 1996. Excitation and inhibition in epilepsy. *The Canadian journal of neurological sciences. Le journal canadien des sciences neurologiques*, **23**(3), 167–74.

Gerstein, George L., & Mandelbrot, Benoit. 1964. Random walk models for the spike activity of a single neuron. *Biophysical journal*, **4**(jan), 41–68.

Haider, Bilal, Duque, Alvaro, Hasenstaub, Andrea R, & McCormick, David a. 2006. Neocortical network activity in vivo is generated through a dynamic balance of excitation and inhibition. *The Journal of neuroscience*, **26**(17), 4535–45.

Higley, Michael J., & Contreras, Diego. 2006. Balanced excitation and inhibition determine spike timing during frequency adaptation. *Journal of Neuroscience*, **26**(2), 448–457.

Holcman, David, & Tsodyks, Misha. 2006. The emergence of Up and Down states in cortical networks. *PLoS computational biology*, **2**(3), e23.

Jones, Kelly E., Campbell, Patrick K., & Normann, Richard A. 1992. A glass/silicon composite intracortical electrode array. *Annals of biomedical engineering*, **20**(4), 423–37.

Kadanoff, Leo, Götze, Wolfgang, Hamblen, David, Hecht, Robert, Lewis, E., Palciauskas, V., Rayl, Martin, Swift, J., Aspens, David, & Kane, Joseph. 1967. Static Phenomena Near Critical Points: Theory and Experiment. *Reviews of Modern Physics*, **39**(2), 395–431.

Krook-Magnuson, Esther, Armstrong, Caren, Oijala, Mikko, & Soltesz, Ivan. 2013. On-demand optogenetic control of spontaneous seizures in temporal lobe epilepsy. *Nature communications*, **4**(jan), 1376.

Lombardi, Fabrizio, Herrmann, Hans, Perrone-Capano, Carla, Plenz, Dietmar, & De Arcangelis, Lucilla. 2012. Balance between Excitation and Inhibition Controls the Temporal Organization of Neuronal Avalanches. *Physical Review Letters*, **228703**(June), 1–5.

McCormick, David A., Connors, Barry W., Lighthall, James W., & Prince, David A. 1985. Comparative electrophysiology of pyramidal and sparsely spiny stellate neurons of the neocortex. *Journal of neurophysiology*, **54**(4), 782–806.

Monier, Cyril, Fournier, Julien, & Frégnac, Yves. 2008. In vitro and in vivo measures of evoked excitatory and inhibitory conductance dynamics in sensory cortices. *Journal of neuroscience methods*, **169**(2), 323–65.

Okun, Michael, & Lampl, Ilan. 2009. Balance of excitation and inhibition. *Scholarpedia*, **4**(8), 7467.

Okun, Michael, Naim, Amir, & Lampl, Ilan. 2010. The subthreshold relation between cortical local field potential and neuronal firing unveiled by intracellular recordings in awake rats. *The Journal of neuroscience*, **30**(12), 4440–8.

Paz, Jeanne T., Davidson, Thomas J., Frechette, Eric S., Delord, Bruno, Parada, Isabel, Peng, Kathy, Deisseroth, Karl, & Huguenard, John R. 2013. Closed-loop optogenetic control of thalamus as a tool for interrupting seizures after cortical injury. *Nature neuroscience*, **16**(1), 64–70.

Petermann, Thomas, Thiagarajan, Tara C, Lebedev, Mikhail a, Nicolelis, Miguel a L, Chialvo, Dante R, & Plenz, Dietmar. 2009. Spontaneous cortical activity in awake monkeys composed of neuronal avalanches. *Proceedings of the National Academy of Sciences of the United States of America*, **106**(37), 15921–6.

Peyrache, Adrien, Dehghani, Nima, Eskandar, Emad N., Madsen, Joseph R., Anderson, William S., Donoghue, Jacob A., Hochberg, Leigh R., Halgren, Eric, Cash, Sydney S., & Destexhe, Alain. 2012. Spatiotemporal dynamics of neocortical excitation and inhibition during human sleep. *Proceedings of the National Academy of Sciences of the United States of America*, **109**(5), 1731–6.

Renart, Alfonso, de, la Rocha Jamie, Bartho, Peter, Hollender, Liad, Parga, Nestor, Reyes, Alex, & Harris, Kenneth D. 2010. The asynchronous state in cortical circuits. *Science*, **327**(Jan), 587–90.

Rudolph, Michelle, Pospischil, Martin, Timofeev, Igor, & Destexhe, Alain. 2007. Inhibition determines membrane potential dynamics and controls action potential generation in awake and sleeping cat cortex. *J Neurosci*, **27**(May), 5280–90.

Schneidman, Elad, Still, Susanne, Berry, Michael J., & Bialek, William. 2003. Network Information and Connected Correlations. *Physical Review Letters*, **91**(23), 3–6.

Schneidman, Elad, Berry, Michael J, Segev, Ronen, & Bialek, William. 2006. Weak pairwise correlations imply strongly correlated network states in a neural population. *Nature*, **440**(7087), 1007–12.

Shadlen, Michael N., & Newsome, William T. 1994. Noise, neural codes and cortical organization. *Current Opinion in Neurobiology*, **4**(4), 569–579.

Shew, Woodrow L, Yang, Hongdian, Yu, Shan, Roy, Rajarshi, & Plenz, Dietmar. 2011. Information capacity and transmission are maximized in balanced cortical networks with neuronal avalanches. *The Journal of neuroscience*, **31**(1), 55–63.

Shimazaki, Hideaki, Amari, Shun-ichi, Brown, Emery N., & Grün, Sonja. 2012. State-Space Analysis of Time-Varying Higher-Order Spike Correlation for Multiple Neural Spike Train Data. *PLoS Computational Biology*, **8**(3), e1002385.

Shu, Yousheng, Hasenstaub, Andrea, & McCormick, David A. 2003. Turning on and off recurrent balanced cortical activity. *Nature*, **423**(6937), 288–93.

Softky, William R., & Koch, Christof. 1993. The highly irregular firing of cortical cells is inconsistent with temporal integration of random EPSPs. *The Journal of neuroscience*, **13**(1), 334–50.

Sporns, Olaf, & Honey, Christopher J. 2006. Small worlds inside big brains. *Proceedings of the National Academy of Sciences of the United States of America*, **103**(51), 19219–20.

Steriade, Mircea, Nuez, Angel, & Amzica, Florin. 1993. Intracellular analysis of relations between the slow (<1 Hz) neocortical oscillation and other sleep rhythms of the electroencephalogram. *J Neurosci*, **13**, 3266–83.

Stevens, Charles F., & Zador, Anthony M. 1998. Input synchrony and the irregular firing of cortical neurons. *Nature neuroscience*, **1**(3), 210–7.

Symonds, Charles. 1959. Excitation and inhibition in epilepsy. *Proceedings of the Royal Society of Medicine*, **52**(6), 395–402.

Tø nnesen, Jan, Sø rensen, Andreas T, Deisseroth, Karl, Lundberg, Cecilia, & Kokaia, Merab. 2009. Optogenetic control of epileptiform activity. *Proceedings of the National Academy of Sciences of the United States of America*, **106**(29), 12162–7.

Truccolo, Wilson, Hochberg, Leigh R., & Donoghue, John P. 2010. Collective dynamics in human and monkey sensorimotor cortex: predicting single neuron spikes. *Nature neuroscience*, **13**(1), 105–11.

Truccolo, Wilson, Donoghue, Jacob A., Hochberg, Leigh R., Eskandar, Emad N., Madsen, Joseph R., Anderson, William S., Brown, Emery N., Halgren, E, & Cash, Sydney S. 2011. Single-neuron dynamics in human focal epilepsy. *Nat Neurosci*, **14**(May), 635–41.

Vogels, Tim P, & Abbott, L F. 2005. Signal propagation and logic gating in networks of integrate-and-fire neurons. *The Journal of neuroscience : the official journal of the Society for Neuroscience*, **25**(46), 10786–95.

Vreeswijk, Carl. van., & Sompolinsky, Haim. 1996. Chaos in Neuronal Networks with Balanced Excitatory and Inhibitory Activity. *Science*, **274**(5293), 1724–1726.

Wilson, Hugh R., & Cowan, Jack D. 1972. Excitatory and inhibitory interactions in localized populations of model neurons. *Biophysical journal*, **12**(1), 1–24.

Wilson, Kenneth G. 1971. Renormalization Group and Critical Phenomena. I. Renormalization Group and the Kadanoff Scaling Picture. *Physical Review B*, **4**(9), 3174–3183.

Wilson, Kenneth G. 1975. The renormalization group: Critical phenomena and the Kondo problem. *Reviews of Modern Physics*, **47**(4), 773–840.

Wilson, Kenneth G. 1979. Problems in Physics with Many Scales of Length. *ScientificAmerican*, 158–179.

Xing, Jing, & Gerstein, George L. 1996. Networks with lateral connectivity. I. dynamic properties mediated by the balance of intrinsic excitation and inhibition. *Journal of Neurophysiology*, **75**(1), 184–199.

Xue, Mingshan, Atallah, Bassam V., & Scanziani, Massimo. 2014. Equalizing excitation–inhibition ratios across visual cortical neurons. *Nature*, **511**(7511), 596–600.

Yizhar, Ofer, Fenno, Lief E, Prigge, Matthias, Schneider, Franziska, Davidson, Thomas J, O'Shea, Daniel J, Sohal, Vikaas S, Goshen, Inbal, Finkelstein, Joel, Paz, Jeanne T, Stehfest, Katja, Fudim, Roman, Ramakrishnan, Charu, Huguenard, John R, Hegemann, Peter, & Deisseroth, Karl. 2011. Neocortical excitation/inhibition balance in information processing and social dysfunction. *Nature*, **477**(7363), 171–8.

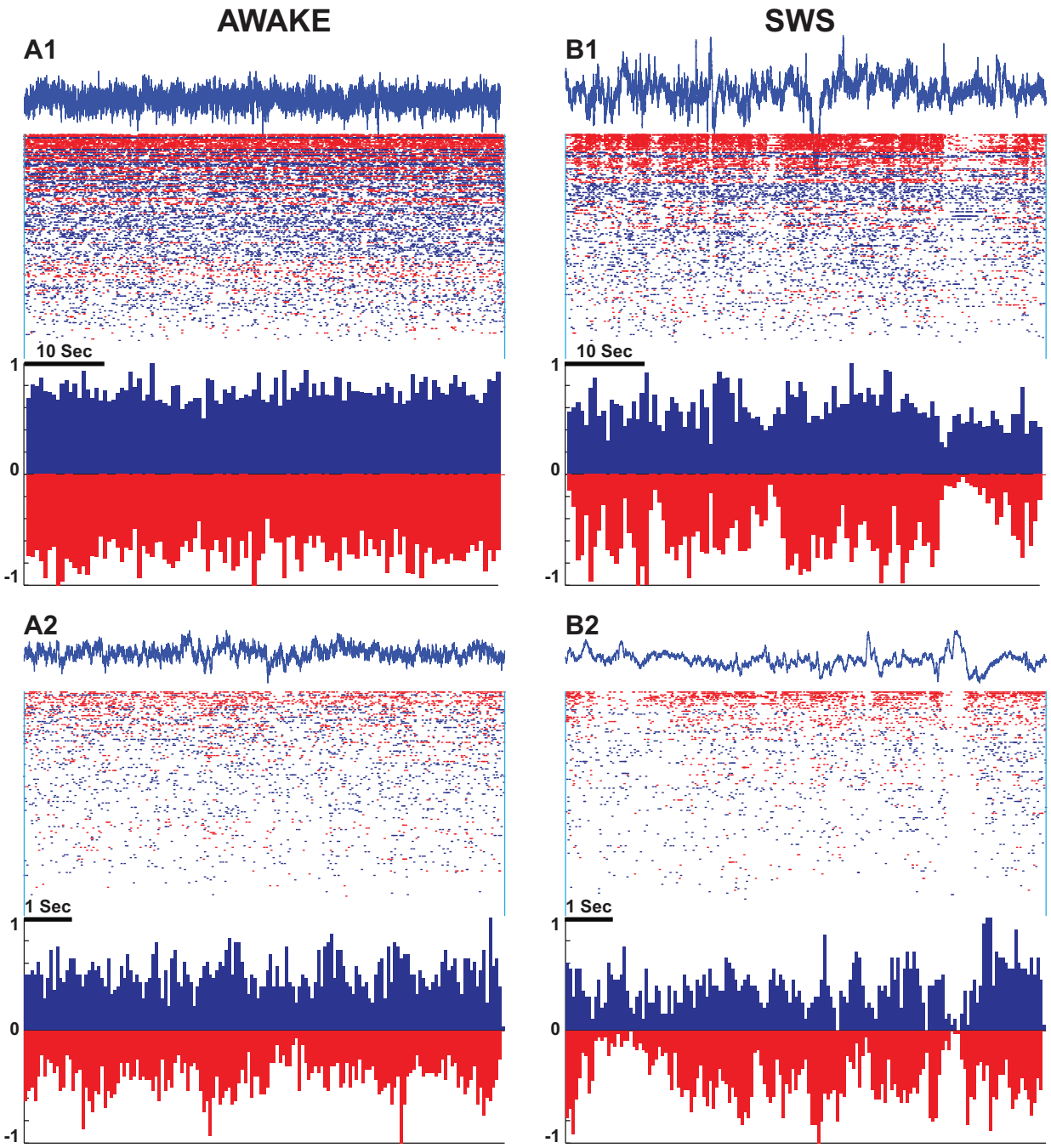


FIG. S1.— Sample recordings for AWAKE (left) and SWS (right) in monkey. A1 and B1 show 60 seconds windows; A2 and B2 show a 10 second window of the same state. In the rasters, putative inhibitory neurons (FS cells) and putative excitatory neurons (RS) are depicted in red and blue, respectively. In each panel, a sample LFP accompanies the spiking activity. Neurons are sorted based on their firing rate within the 60 sec epochs, in a descending order. Histograms show the overall excitatory activity normalized to the maximum of firing rate (within FS or RS category) in the shown example.

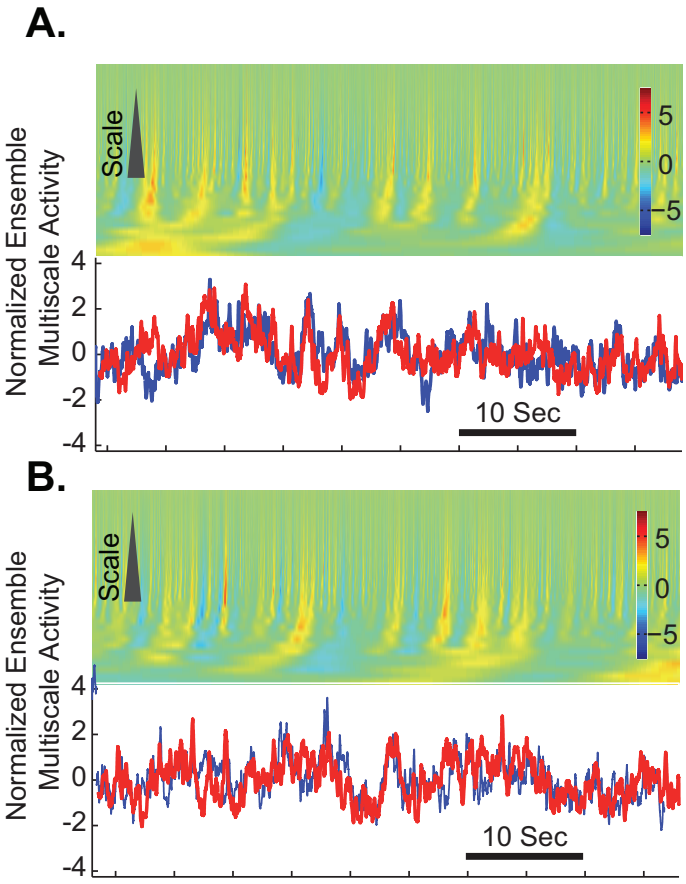


FIG. S2.— Multiscale features of excitation and inhibition balance in two sample recordings from the monkey. As in Fig.3, each row in the heatmap shows the normalized (zscore) difference of ensemble excitation and inhibition for a given scale. The scales are defined as in Fig.4, increasing from the top to bottom (from fine-grain to coarse-grain). The color saturation towards red signifies instantanous dominance of inhibition. Blue saturation shows instantanous dominance of excitation, while green shows tight match between normalized ensemble excitation and inhibition. Line traces show the zscored addition of normalized excitatory (blue) and inhibitory (red) ensembles across the scales.

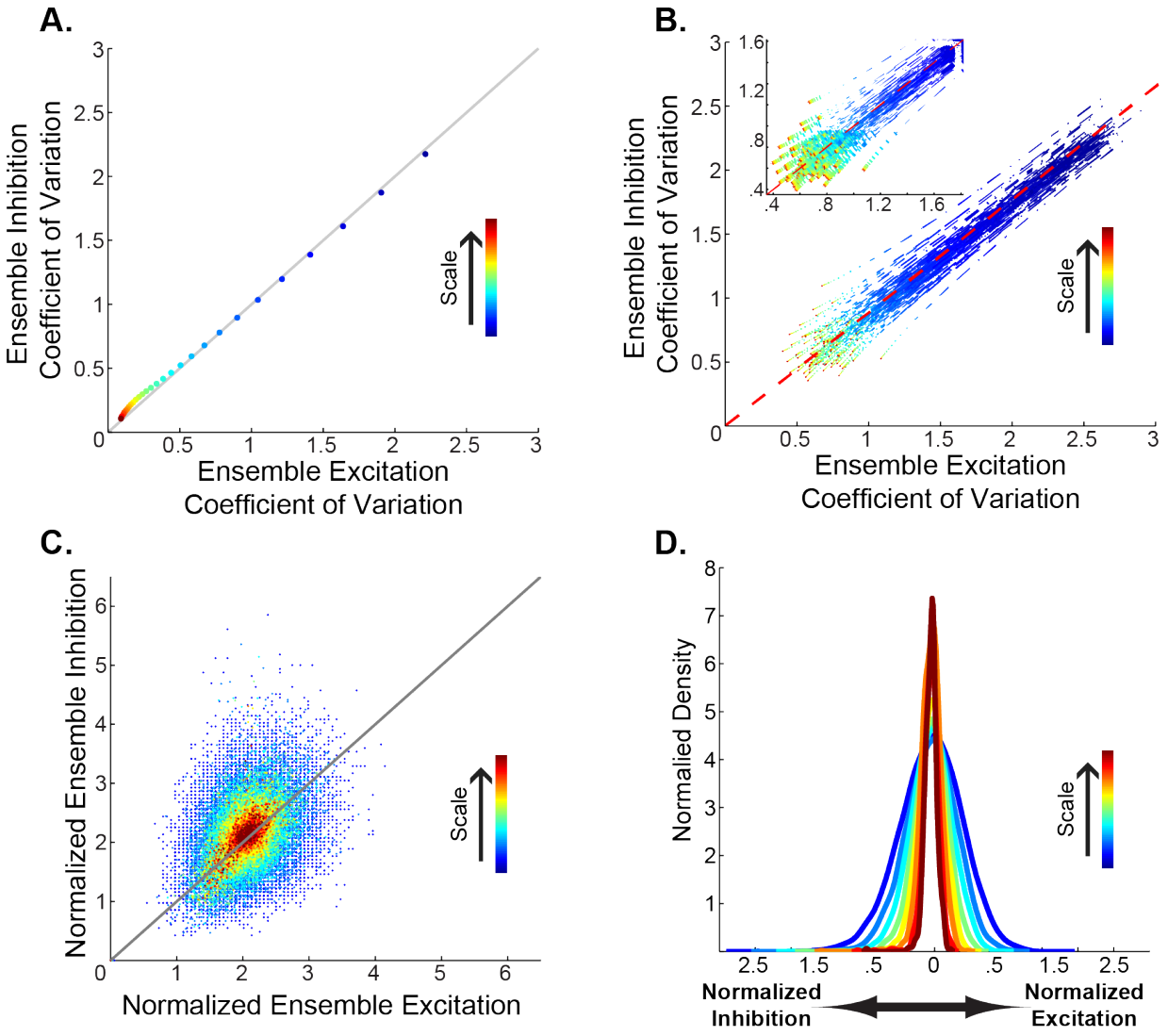


FIG. S3.— A. Multiscale coefficient of variation (CV) of ensemble excitation vs inhibition. The distribution of CV across scales stays close to the diagonal, representing that the fluctuation around the mean for both ensembles stay in the same range. B. Multiscale CV of 100 realization of surrogate data (phase randomized), show that the two fluctuation around the mean of the two ensembles do not follow the same trend (in both the extent and alignment on the diagonal) as of the raw data. C. Dispersion of the E-I ensemble pairs at multiple scales show a unidirectional symmetry suggestive of an overall balance (also see Fig.6B and Fig.7A). C, D. The dispersion from the diagonal is reduced as one moves toward coarse-grained scales (see also Fig.6B). and Fig.S5C).

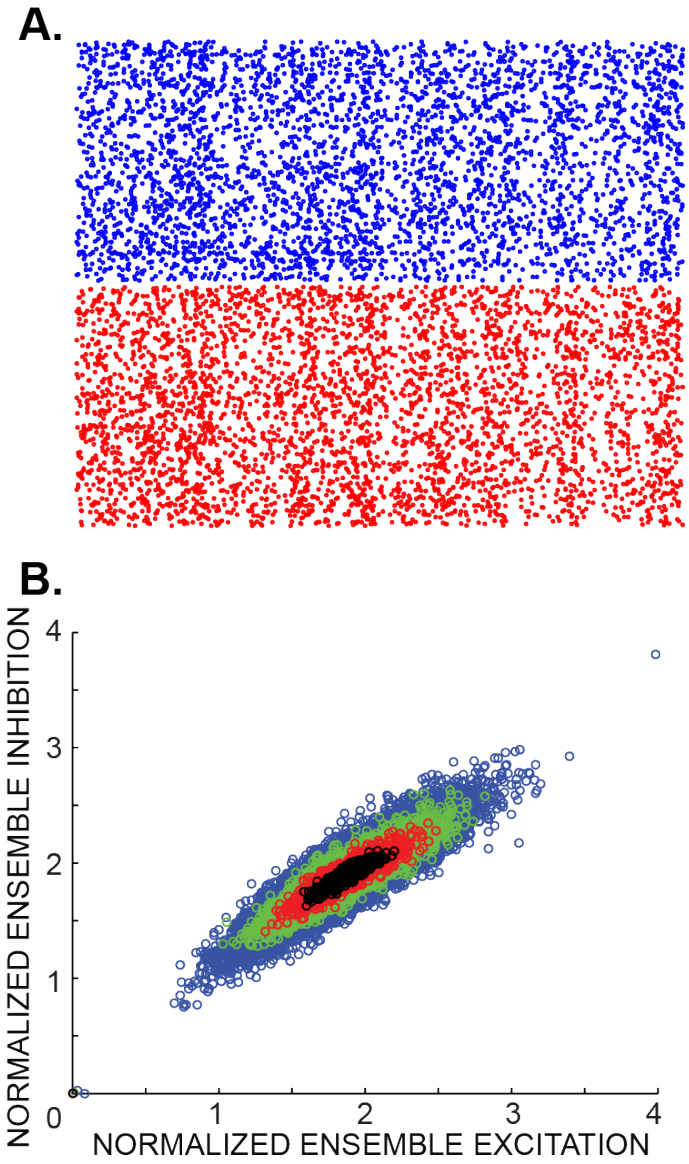


FIG. S4.— A. Raster of 2000 excitatory (blue) and 2000 inhibitory (red) in a COBA (conductance-based) model, showing AI (asynchronous irregular) state. Panel B shows the scatter plot of normalized ensemble excitation and inhibition for times $t_1$ to $t_n$, with n representing the length of the time series at a given scale. Blue, red, green and black represent sample scales (scales 7, 11 and 15 according to Fig.4A). Similar to the experimental data, the paired E-I data scatter along the diagonal line, representing an overall balance across multiple scales, with moment to moment dominance of E or I, while the degree of scattering along the diagonal shrinks with coarse-graining (as as in Fig.6B). (for more details see also Fig.S5).

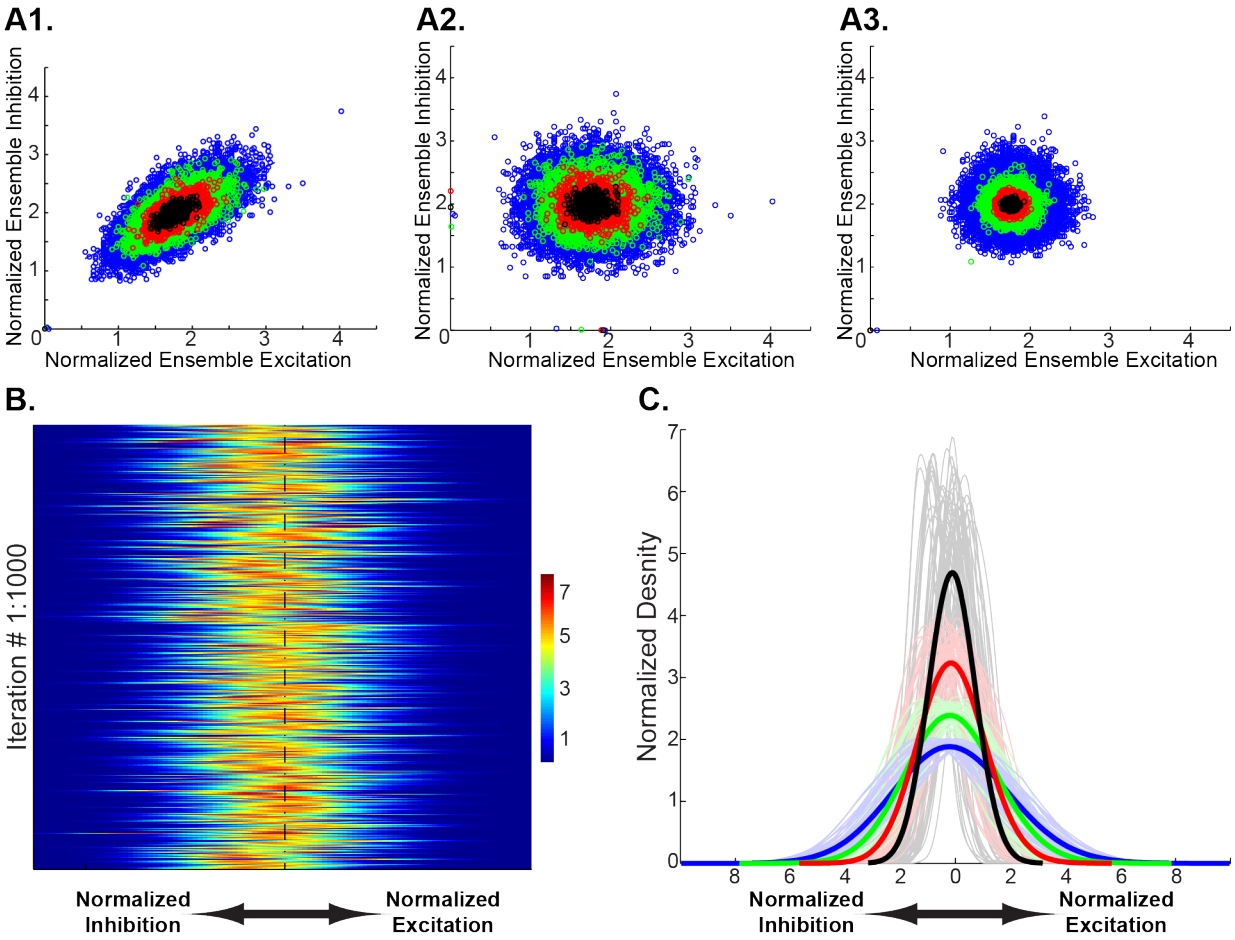


FIG. S5.— Multiscale features of balance in subsampled set of AI model (N=600). A1. Scatter plot of normalized ensemble excitation and inhibition for times $t_1$ to $t_n$, with n representing the length of the time series at a given scale. Blue, red, green and black represent the different scales as shown in Fig.6. Similar to the experimental data, the paired E-I data scatter along the diagonal line, representing an overall balance across multiple scales, with moment to moment dominance of E or I, while the degree of scattering along the diagonal shrinks with coarse-graining (as as in Fig.6B and Fig.S3C,D). The effects of randomization are shown in A2 (Random permutation of ISI in the ensemble series), and A3 (Circular shift of spike ensemble). For details see methods. Randomization deconstruct the alignment of ensemble E-I pairs along the diagonal line and creates white noise. Panel B. shows a monte carlo simulation where each row is one iteration of subsampling 600 cells from the 2000 simulated pool of neuron in each ensemble category for an example scale. The heatmap shows that even with subsampling, the instantaneous dominance of excitation or inhibition in light of the overall balance is still a robust feature. In panel C, 50 realization of such instantaneous dominance (as in Fig.6B) are shown for the 4 example scales in A.

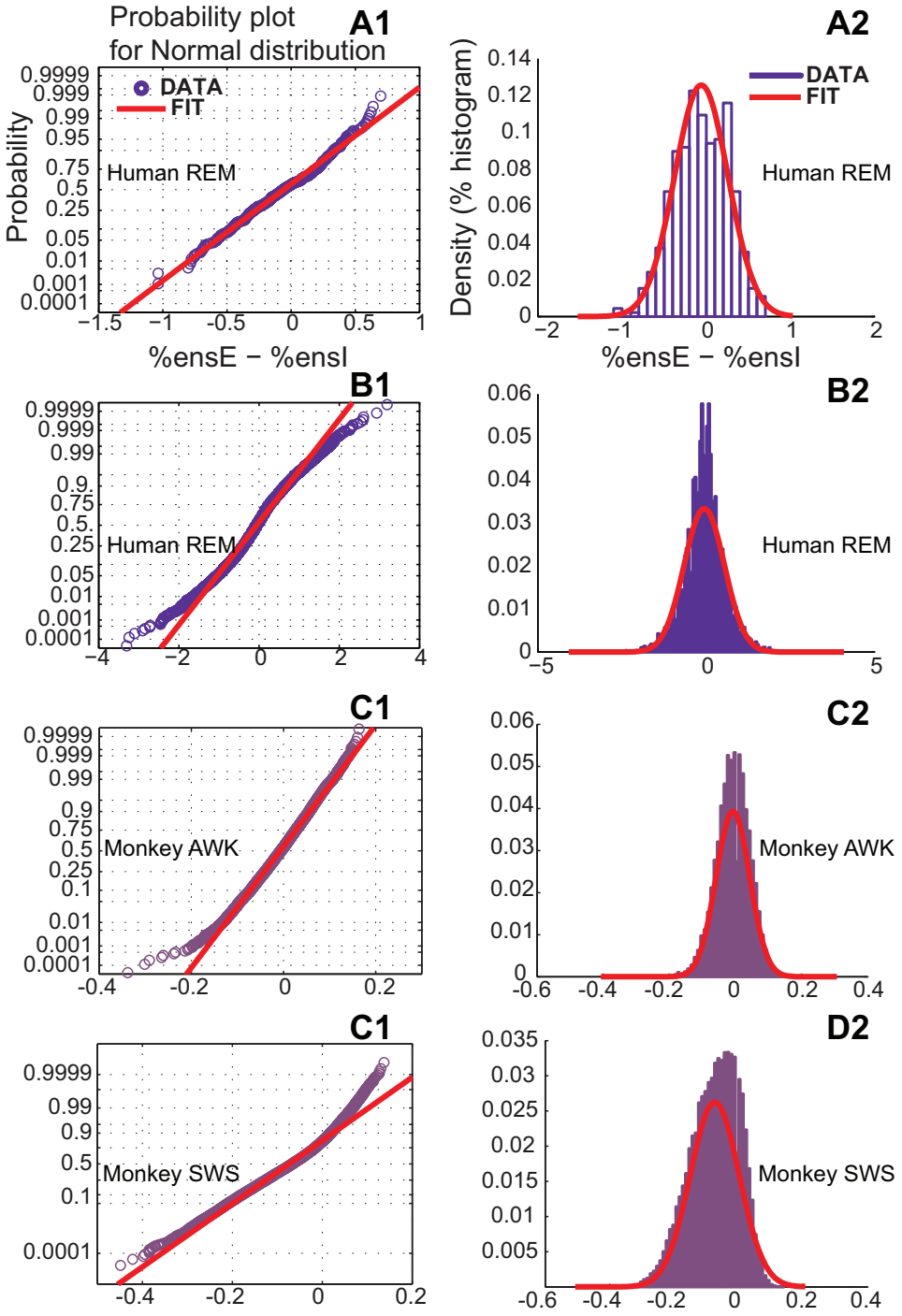


FIG. S6.— Panels in the left show normal probability plot of ensemble excitation and ensemble inhibition difference for, two sample scales from the same state (REM) in a human subject (A1 and B1) as well as two similar scales from different states (AWAKE and SLEEP) in monkey. Panels in the right show corresponding kernel density and histogram of ensemble difference. One can notice that although qualitative balance is noticeable, as in Fig.6, deviations from perfect normality is too an aspect of the system (tails of the distributions deviate from the straight line in red). As shown here, in some scales, deviation from perfect symmetry is different from scale to scale.

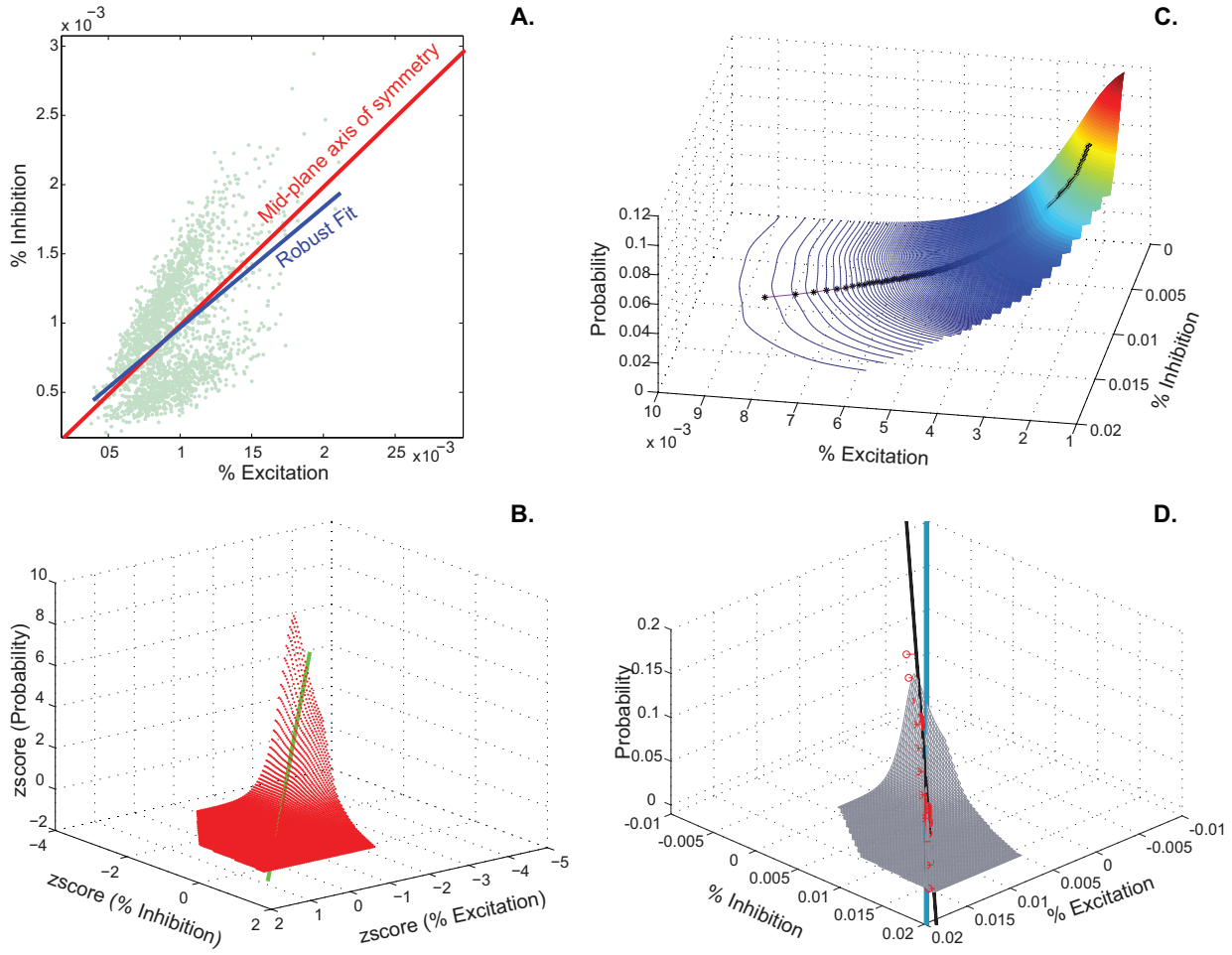


FIG. S7.— Panel A shows estimation of deviation from balance, between ensemble excitation and inhibition for a sample scale of SWS in a human subject, using robust bisquare regression. The fit (blue line) to the green cloud (data) shows the axis of symmetry of the data. Its deviation from the symmetry axis of the plane (in red) shows the degree of balance deviation. Panels B to D each show a different method for estimating the deviation from perfect symmetry. Panel B, shows the major orientation axis of the Zscored data. Panel C, shows the distribution of E-I ensemble fraction pairs for a sample scale during SWS. The black lines are the centroids of the iso-surfaces. Panel D, combining these info, one can find the mid-plane of the data (shown in black) and find its tetrahedral angle with the plane of absolute symmetry (shown in cyan). The distribution of such angles is shown in Fig.8.

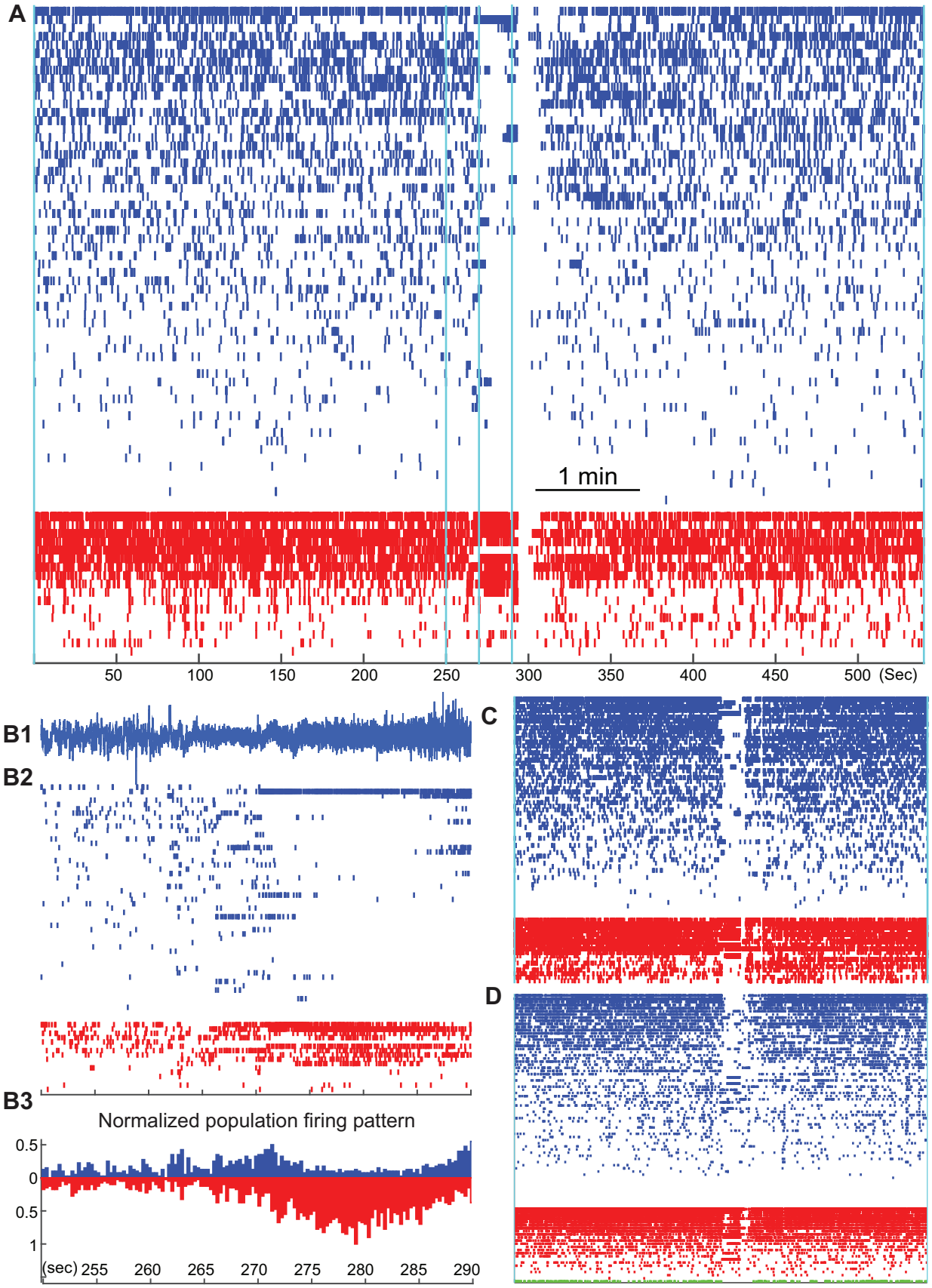


FIG. S8.— Misbalance in more example seizure recordings in human. Panel A shows a 9 minute recording. Panels in B are the zoomed in version (the middle 40 seconds) of the same epoch (shown with the vertical lines in A). RS cells are in blue and ranked based on their firing rate within this epoch. Red cells show FS cells and are ordered according to their class firing rate. B1, LFP activity in the zoomed period, corresponding to B2 raster of FS and RS cells. B3, Normalized mirrored histogram showing where the misbalance occurs. C, D. Two additional seizures similar to panel A (Note on panel D: in this patient, one unit was not categorized as either FS or RS, shown in green). Seizure happens around the mid-point and is visually distinct from the rest of the recording.